

DOI 10.24425/ae.2020.133915

Application of fractional calculus in iterative sliding mode synchronization control

XIN ZHANG^{1,2}, WEN-RU LU¹ , LIANG ZHANG¹, WEN-BO XU¹

¹*School of Automation & Electrical Engineering of Lanzhou Jiaotong University
Lanzhou, 730070, China*

²*Gansu Provincial Engineering Research Center for
Artificial Intelligence and Graphics and Image Processing
China*

e-mail: 1115682030@qq.com

(Received: 01.10.2019, revised: 25.02.2020)

Abstract: In order to control joints of manipulators with high precision, a position tracking control strategy combining fractional calculus with iterative learning control and sliding mode control is proposed for the control of a single joint of manipulators. Considering the coupling between joints of manipulators, a fractional-order iterative sliding mode cross-coupling control strategy is proposed and the theoretical proof of its progressive stability is given. The paper takes a two-joint manipulator as the research object to verify the control strategy of a single-joint manipulator. The results show that the control strategy proposed in this paper makes the two-joint mechanical arm chatter less and the tracking more accurate. The synchronous control of the manipulator is verified by a three-joint manipulator. The results show that the angular displacement adjustment times of the three-joint manipulator are 0.11 s, 0.31 s and 0.24 s, respectively. 3.25 s > 5 s, 3.15 s of a PD cross-coupling control strategy; 2.85 s, 2.32 s, 4.22 s of a PD iterative cross-coupling control strategy; 0.14 s, 0.33 s, 0.28 s of a fractional-order sliding mode cross-coupling control strategy. The root mean square error of the position error of the designed control strategy is 6.47×10^{-6} rad, 3.69×10^{-4} rad, 6.91×10^{-3} rad, respectively. The root mean square error of the synchronization error is 3.96×10^{-4} rad, 1.36×10^{-3} rad, 7.81×10^{-3} rad, superior to the other three control strategies. The results illustrate the effectiveness of the proposed control method.

Key words: cross-coupling control, fractional calculus, iterative learning control, PD control, robot arm, sliding mode control



© 2020. The Author(s). This is an open-access article distributed under the terms of the Creative Commons Attribution-NonCommercial-NoDerivatives License (CC BY-NC-ND 4.0, <https://creativecommons.org/licenses/by-nc-nd/4.0/>), which permits use, distribution, and reproduction in any medium, provided that the Article is properly cited, the use is non-commercial, and no modifications or adaptations are made.

1. Introduction

A manipulator is a complex and versatile multi-input and multi-output complex system with non-linear and time-varying uncertainties [1]. It is widely used in anti-terrorism and explosion-proof industrial assembly and other fields for the character of the variety of types and the flexibility of operation.

It is found that iterative learning combined with sliding mode control can enhance the robustness of the system and suppress the chattering of the system to improve the control precision of the manipulator, which can solve the problem of poor robustness of the iterative learning control strategy [2] and the accuracy of the sliding mode control strategy which are caused by the chattering phenomenon in the control process [3, 4]. In [5], an iterative sliding mode controller is designed, which uses the advantage of invariance of variable structure control for system parameters and external disturbances and the advantage of an iterative learning control strategy which need not depend on the accurate mathematical model to improve the stability of the control system and Dynamic Response. In [6], a multi-cycle iterative sliding mode control algorithm to improve the control accuracy of linear motors is proposed. In [7], the iterative learning control and sliding mode control are used to study the satellite attitude fault tolerance control with external disturbance.

In recent years, fractional calculus has been widely used in signal processing, control, biomedicine, and electrical engineering [8]. The fractional order control system is widely used in fractional order sliding integral control and fractional order iterative learning control for its memory and heritability [9]. In [10], the robustness of the fractional order iterative learning control algorithm is discussed. When the system is disturbed by external bounded noise, the algorithm can ensure that the tracking error of the system is uniformly bounded with the increased number of iterations. In [11], an effective fractional sliding mode control method is proposed and the good performance of the controller is verified.

For multi-degree-of-freedom industrial robots, synchronous control refers to the coordination of multiple variables, and the variables involved are generally position and velocity. In [12, 13], first proposed the cross-coupled control idea and applied to the traditional machining device. In the synchronous control system of the two-axis motion system, the information of other related axes is introduced when controlling the single-axis motion to achieve the synchronization. In [14], a cross-coupling control algorithm based on contour error is proposed, which can realize high-precision tracking of arbitrary trajectories by robots. In [15], the synchronization control of the precise position of adjacent axes is realized by combining global sliding mode control with a cross-coupling control strategy.

There are two control strategies respectively proposed in this paper based on the above studies. One is the position tracking control strategy, which combines fractional calculus control and iterative sliding mode control of a single-joint mechanical arm for better robustness and engineering practicability of a multi-axis synchronous system, the other is the fractional-order iterative sliding mode cross-coupling control strategy, which considers the coupling relationship between the joints of the arms. The effectiveness and feasibility of the single-joint and multi-joint synchronization control strategies are verified by the comparison with other control strategies.

2. Basic theory

The definition of the Caputo fractional integral type is as follows [16]:

$${}_a D_t^\alpha f(t) = \frac{1}{\Gamma(m-\alpha)} \int_a^t \frac{f^{(m)}(\tau)}{(t-\tau)^{\alpha-m+1}} dt, \quad m-1 < \alpha \leq m, \quad (1)$$

where: m is the smallest integer greater than α and $\Gamma(\cdot)$ is the Gamma function. To simplify expression, use D^α instead of ${}_a D_t^\alpha$.

Correctly state lemma 1 as specified in reference [17].

Let $x = 0$ be an equilibrium point for the non-autonomous fractional-order system:

$$D^\alpha x(t) = f(x, t), \quad (2)$$

if $x = 0$ is the fractional-order non-equilibrium autonomous system, and $f(x, t)$ satisfies the Lipschitz condition. Assume a Lyapunov function $V(t, x(t))$ which satisfies the following conditions:

$$\alpha_1 \|x\| \leq V(t, x) \leq \alpha_2 \|x\|, \quad \dot{V}(t, x) \leq -\alpha_3 \|x\|, \quad (3)$$

where: α_1, α_2 and α_3 are positive numbers, $\beta \in (0, 1)$. Then system (2) is progressively stable.

The basic idea of iterative learning control is as follows: if the condition of a desired output $y_d(t)$ and the initial running state of each $x_k(0)$ are given, repeat the calculation more times according to a certain algorithm in a certain time of t until the control input $u_k(t)$ is close to $u_d(t)$ and the output $y_k(t)$ approaches $y_d(t)$. In this paper, closed-loop learning control is used:

$$\mathbf{u}_{k+1}(t) = L(\mathbf{u}_k(t), e_{k+1}(t)), \quad (4)$$

where: L is the nonlinear operator and $e_k(t)$ is the tracking error.

3. Fractional order iterative sliding mode reaching law

Approaching motion is an important part of the sliding mode motion, the movement mode of which is a process where the system gradually approaches the switching surface from the arbitrary initial position until it reaches the switching surface. A reasonable reaching law can get better dynamic quality in the approach process by accelerating the speed of the approach to a large extent and by reducing the chattering of the system. In the traditional sliding mode control theory, the most popular reaching law is the exponential approach law, but its buffeting phenomenon is obvious and the approach speed is slow [18]. This paper designs a fractional order reaching law:

$$D^\beta s = -k \operatorname{sgn}(s), \quad (5)$$

where: $0 < \beta < 1$ and D represents the calculus operators.

3.1. Reaching law buffeting analysis

Take the traditional exponential reaching law as an example:

$$\dot{s} = -\varepsilon \operatorname{sgn}(s) - ks, \quad 0 < \varepsilon, \quad k > 0. \quad (6)$$

When s approaches 0, its limit on the sliding surface is:

$$\lim_{s \rightarrow 0} \dot{s} = \begin{cases} -\varepsilon & s \rightarrow 0^+ \\ \varepsilon & s \rightarrow 0^- \end{cases}. \quad (7)$$

It can be obtained from (6) that when s approaches zero, the system will chatter with amplitude near the equilibrium point. For reaching law (5) designed in this paper, when $s \rightarrow 0^+$ and $s \rightarrow 0^-$, there always is $\dot{s} = 0$, which indicates that the system has no chattering phenomenon near the steady state.

3.2. Reaching rate analysis

Proposition 1

Based on the choice of the power term β , the reaching time in fractional reaching law can be shorter than the reaching time in exponential reaching law.

Proof

The approach rate of the fractional reaching law is greater than the exponential reaching law when $\dot{s} > 0$.

1. The approach time of the exponential reaching law

It can be obtained from (6):

$$dt = \frac{ds}{-\varepsilon \operatorname{sgn}(s) - ks}. \quad (8)$$

When $s > 0$:

$$t'_1 = \int_0^s \frac{ds}{-\varepsilon \operatorname{sgn}(s) - ks} = \int_0^s \frac{ds}{-\varepsilon - ks} = -\frac{1}{k} \left[\ln \left(1 + \frac{k}{\varepsilon} s \right) \right]. \quad (9)$$

When $s < 0$:

$$t'_2 = \int_0^{-s} \frac{ds}{-\varepsilon \operatorname{sgn}(s) - ks} = \int_0^{-s} \frac{ds}{\varepsilon - ks} = -\frac{1}{k} \left[\ln \left(1 + \frac{k}{\varepsilon} s \right) \right]. \quad (10)$$

When $s = 0$, that is on the slip surface, $t'_3 = 0$.

So the approach time of the exponential reaching law is:

$$t' = \begin{cases} -\frac{1}{k} \left[\ln \left(1 + \frac{k}{\varepsilon} s \right) \right], & s \neq 0 \\ 0, & s = 0 \end{cases}. \quad (11)$$

2. The approach time of the fractional order reaching law

It can be obtained from references [19, 20]:

$$J^\partial D^\partial s = J^\partial(-k \operatorname{sgn}(s)), \quad J^\partial f(t) = \frac{1}{\Gamma(\partial)} \int_0^t (t-\tau)^{\partial-1} f(\tau) d\tau. \quad (12)$$

The simplified expression is $s(t) - s(0) = J^\partial(-k \operatorname{sgn}(s))$ applying a standard derivate:

$$\frac{ds}{dt} = -k D J^\partial(-\operatorname{sgn}(s)), \quad J^\partial 1 = \frac{t^\partial}{\Gamma(1+\partial)}. \quad (13)$$

From Equations (13):

$$t^\partial dt = \frac{\Gamma(1+\partial)}{k D \operatorname{sgn}(s)} ds \Rightarrow t^{\partial+1} = \frac{\Gamma(1+\partial)}{k D \operatorname{sgn}(s)(\partial+1)} ds. \quad (14)$$

The approach time of the fractional order reaching law is:

$$\begin{cases} t = \sqrt[\partial+1]{\frac{\Gamma(1+\partial)s}{k D(\partial+1)}}, & s \neq 0 \\ 0, & s = 0 \end{cases}. \quad (15)$$

It can be obtained from (11) and (15):

$$\begin{cases} t' - t = \frac{\ln\left(1 + \frac{k}{\varepsilon}s\right)}{-k} - \frac{\Gamma(1+\partial)s}{k D(\partial+1)} = \frac{\ln\left(\frac{\varepsilon \cdot e^{(-k) \cdot \sqrt[\partial+1]{\frac{\Gamma(1+\partial)s}{k D(\partial+1)}}}}{\varepsilon + ks}\right)}{k} > 0, & s \neq 0 \\ 0, & s = 0 \end{cases}. \quad (16)$$

It can be concluded from the above derivation that the approach rate of the fractional reaching law is higher than the approach rate of the exponential reaching law.

3.3. Stability analysis

Use the Lyapunov function:

$$V(t) = \frac{1}{2} s^T s. \quad (17)$$

According to the definition of the Caputo type fractional calculus in (1),

$$\begin{cases} \dot{s} > 0 \\ \dot{s} < 0 \end{cases} \Rightarrow \begin{cases} D^\alpha s > 0 \\ D^\alpha s < 0 \end{cases}. \quad (18)$$

Take the derivative of (17), and combine with the fractional order reaching law of (18):

$$\dot{V}(t) = s^T \dot{s} = s^T D^{1-\alpha}(-k \operatorname{sgn}(s)). \quad (19)$$

The following can be obtained by $\text{sgn}(D^{1-\alpha}(-k \text{sgn}(s))) = -k \text{sgn}(s)$ [21]:

$$\text{sgn}(\dot{V}(t)) = \text{sgn}(s^T) \text{sgn}(D^{1-\alpha}(-k \text{sgn}(s))) = -k \text{sgn}(s^T) \text{sgn}(s) = -k. \quad (20)$$

Then $\dot{V} \leq 0 \Rightarrow D^\alpha V \leq 0$, the selected fractional order reaching law is progressively stable.

4. Single joint tracking control strategy

The nominal model of an n -joint arm is as follows:

$$M(q)\ddot{q} + C(q, \dot{q})\dot{q} + G(q) = \tau + f(t), \quad (21)$$

where: $q \in \mathbf{R}^n$ represents the joint position of the manipulator, $\dot{q} \in \mathbf{R}^n$ and $\ddot{q} \in \mathbf{R}^n$, respectively, represent the velocity vector and acceleration vector of the mechanical arm joint, $M(q) \in \mathbf{R}^{n \times n}$ represents the inertia matrix, $C(q, \dot{q}) \in \mathbf{R}^{n \times n}$ represents the centrifugal force and the Coriolis force matrix, $G(q) \in \mathbf{R}^n$ represents the gravity term, $\tau \in \mathbf{R}^n$ represents the control torque and $f(t)$ represents the uncertain disturbance term.

4.1. Design of control law

According to the dynamic model of the manipulator, $q_d(t)$ is the ideal position of the joint, $q(t)$ is the actual position of the joint, and the tracking error of each joint position is:

$$e(t) = q_d(t) - q(t). \quad (22)$$

Take the second derivative of (22):

$$\dot{e} = \dot{q}_d - \dot{q}. \quad (23)$$

Take the sliding surface as:

$$s = ce + \dot{e}. \quad (24)$$

Take the derivative of (24):

$$\dot{s} = c\dot{e} + \ddot{e}. \quad (25)$$

Substitute (21) and (22) into (25):

$$\dot{s} = c\dot{e} + \ddot{q}_d - M^{-1}[\tau - G - C\dot{q} + f(t)]. \quad (26)$$

The reaching law takes the fractional order reaching law designed above:

$$D^\alpha s = -k \text{sgn}(s). \quad (27)$$

Take the derivative of (27):

$$\dot{s} = D^{1-\alpha}(-k) \text{sgn}(s). \quad (28)$$

The control law can be obtained by combining (26) with (28),

$$u_{k+1}(t) = u_k(t) + M[\ddot{q}_d + c\dot{e} + kD^{1-\alpha} \text{sgn}(s)] + G + C\dot{q} - f. \quad (29)$$

4.2. Verification of controller validity

Taking the two-joint manipulator as an example, the numerical simulation was completed by the toolbox of FOMCON [22]. The set number of iterations is 10, the second joint position command is $q_{1d} = \sin(3t)$, $q_{2d} = \cos(3t)$. The following control methods are compared and analyzed by simulation method 1: fractional-order iterative sliding mode control; method 2: fractional-order sliding mode control; method 3: integer-order iterative sliding mode control.

The single joint control system control block diagram is shown in Fig. 1. In the figure, $u_k(t)$ and $u_{k+1}(t)$ are the signals of the previous control and the current control; $y_r(t)$ and $y_{k+1}(t)$ are the input signals and feedback signals; $e_k(t)$ is the error.

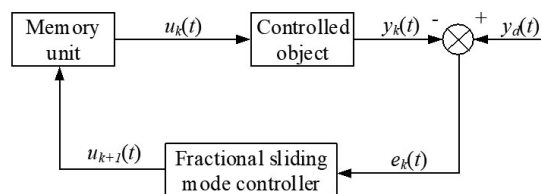


Fig. 1. System control block diagram

4.3. Simulation

Fig. 2 shows curves of the control input for the system in methods 1–2. It can be seen that the chattering of the sliding mode control is better suppressed and the control input signal becomes smoother via the combination of the iterative learning control algorithm and the fractional calculus. Fig. 3 shows the maximum absolute value convergence curve of the position (speed)

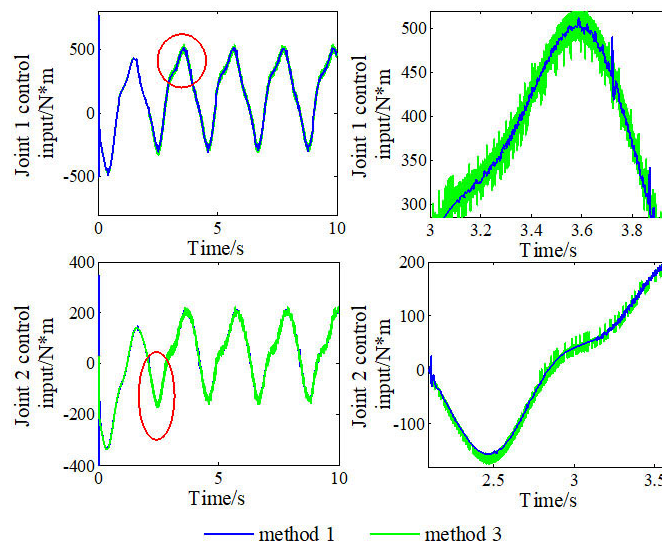


Fig. 2. Control input curve

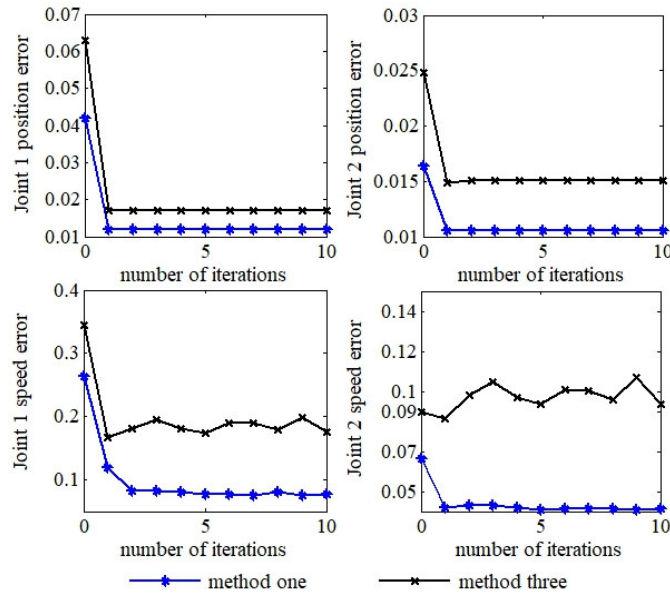


Fig. 3. Error norm convergence process

error of the two joints in methods 1, 3, and Table 1 and Table 2 contain their data comparisons, respectively. It can be concluded that method 1 has smaller position and velocity errors as well as higher control precision than method 3.

Table 1. Comparison of position error

| | | Maximum value | Minimum value |
|--------------|---------|---------------|---------------|
| Method one | Joint 1 | 0.0667 | 0.0407 |
| | Joint 2 | 0.2645 | 0.0757 |
| Method three | Joint 1 | 0.1070 | 0.0939 |
| | Joint 2 | 0.3452 | 0.1761 |

Table 2. Comparison of speed error

| | | Maximum value | Minimum value |
|--------------|---------|---------------|---------------|
| Method one | Joint 1 | 0.0164 | 0.0106 |
| | Joint 2 | 0.0421 | 0.0119 |
| Method three | Joint 1 | 0.0248 | 0.0150 |
| | Joint 2 | 0.0629 | 0.0171 |

5. Fractional-order iterative sliding mode cross-coupling synchronization control strategy

5.1. Definition of synchronization control strategy

Define the difference between tracking errors of two adjacent axes as the synchronization error:

$$\varepsilon_1 = e_1 - e_2, \quad \dots, \quad \varepsilon_i = e_i - e_{i+1}, \quad \varepsilon_n = e_n - e_1, \quad (30)$$

where ε_i is the synchronization error of the i -th axis. Let $\varepsilon_{(t)} = [\varepsilon_1(t), \varepsilon_2(t), \dots, \varepsilon_n(t)]^T$ be the synchronization error vector, so:

$$\varepsilon = T e. \quad (31)$$

Define the coupling error as:

$$E = e + a\varepsilon, \quad (32)$$

where a is the positive fixed matrix representing the control gain of the coupling error.

Substitute (31) into (32):

$$E = (I + aT) e. \quad (33)$$

It is obvious that when the coupling error converges to 0, the position error and synchronization error of the system also converge to 0, thereby achieving the purpose of synchronous control.

5.2. Design of controller

In this paper, a control method of position error and coupling error separation is selected. The position control of the single joint adopts the iterative sliding mode controller which was mentioned above, and the coupling error is compensated by designing a PD synchronous controller. Based on Equation (31) and $e_i = q_{di} - q_i$ the following can be obtained:

$$\dot{e} = -\dot{q}, \quad \dot{\varepsilon} = T\dot{e} = -T\dot{q}. \quad (34)$$

Design a PD-based synchronous controller based on cross-coupling:

$$u_\Delta = K_P E + K_D \dot{E} + (I + aT)^{-1} K_e \dot{e}. \quad (35)$$

where K_P represents the proportional gain, K_D represents the differential gain, and K_e represents the compensation gain. The third function on the right side of (35) is to ensure the stability of the system. Substitute (35) into (21):

$$M(q)\ddot{q} + C(q, \dot{q})\dot{q} = K_P E + K_D \dot{E} = (I + aT)^{-1} K_e \dot{e}. \quad (36)$$

Analysis of stability:

Theorem 1

When the following conditions are met, the controller designed in this paper can ensure that both the position error and the synchronization error converge to zero with time, that is when $t \rightarrow \infty, e \rightarrow 0, \varepsilon \rightarrow 0$.

1. The control gain is small enough.

2. The compensation gain \mathbf{K}_e satisfies the condition of

$$\lambda_{\min}\{\mathbf{K}_e\} = C_1 \|\mathbf{q}\| + C_2 \|\dot{\mathbf{q}}\| \geq c_1 \|\mathbf{q}\| + c_2 \|\dot{\mathbf{q}}\|,$$

where $\lambda_{\min}\{\mathbf{K}_e\}$ is the minimum eigenvalue of \mathbf{K}_e , C_1 and C_2 are both normal numbers, and c_1 and c_2 are both Lipschitz constants.

Proof

Use the following function:

$$V = \frac{1}{2} \left(\dot{\mathbf{e}}^T \mathbf{M}(\mathbf{q}) \dot{\mathbf{e}} + \mathbf{a} \dot{\mathbf{e}}^T \mathbf{T} \mathbf{M}(\mathbf{q}) \dot{\mathbf{e}} \right) + \frac{1}{2} \mathbf{E}^T \mathbf{K}_P \mathbf{E}. \quad (37)$$

If the control gain α is sufficiently small and

$$\mathbf{M}(\mathbf{q}) \dot{\mathbf{e}} + \mathbf{a} \dot{\mathbf{e}}^T \mathbf{T} \mathbf{M}(\mathbf{q}) \dot{\mathbf{e}} \geq 0,$$

then (37) is a positive definite function. Take the derivative of V :

$$\dot{V} = \dot{\mathbf{e}}^T (\mathbf{I} + \mathbf{a} \mathbf{T}) \mathbf{M}(\mathbf{q}) \ddot{\mathbf{e}} + \frac{1}{2} \dot{\mathbf{e}}^T (\mathbf{I} + \mathbf{a} \mathbf{T}) \dot{\mathbf{M}}(\mathbf{q}) \dot{\mathbf{e}} + \mathbf{E}^T \mathbf{K}_P \dot{\mathbf{E}}. \quad (38)$$

(36) is simultaneously multiplied by $\dot{\mathbf{E}}^T$ on both sides to obtain:

$$\dot{\mathbf{E}}^T \mathbf{M}(\mathbf{q}) \ddot{\mathbf{q}} + \dot{\mathbf{E}}^T \mathbf{C}(\mathbf{q}, \dot{\mathbf{q}}) \dot{\mathbf{q}} = \dot{\mathbf{E}}^T \mathbf{K}_P \mathbf{E} + \dot{\mathbf{E}}^T \mathbf{K}_D \dot{\mathbf{E}} + \dot{\mathbf{E}}^T (\mathbf{I} + \mathbf{a} \mathbf{T})^{-1} \mathbf{K}_e \dot{\mathbf{e}}. \quad (39)$$

According to $\mathbf{E} = (\mathbf{I} + \mathbf{a} \mathbf{T}) \mathbf{e}$ and (34), (39) can be written as:

$$-\dot{\mathbf{e}}^T (\mathbf{I} + \mathbf{a} \mathbf{T}) \mathbf{M}(\mathbf{q}) \ddot{\mathbf{q}} - \dot{\mathbf{e}}^T (\mathbf{I} + \mathbf{a} \mathbf{T}) \mathbf{C}(\mathbf{q}, \dot{\mathbf{q}}) \dot{\mathbf{e}} = \dot{\mathbf{E}}^T \mathbf{K}_P \mathbf{E} + \dot{\mathbf{E}}^T \mathbf{K}_D \dot{\mathbf{E}} + \dot{\mathbf{e}}^T \mathbf{K}_e \dot{\mathbf{e}}. \quad (40)$$

Substitute (40) into (38) and obtain:

$$\begin{aligned} \dot{V} &= \dot{\mathbf{e}}^T (\mathbf{I} + \mathbf{a} \mathbf{T}) \left(\frac{1}{2} \dot{\mathbf{M}}(\mathbf{q}) - \mathbf{C}(\mathbf{q}, \dot{\mathbf{q}}) \right) \dot{\mathbf{e}} - \dot{\mathbf{E}}^T \mathbf{K}_D \dot{\mathbf{E}} - \dot{\mathbf{e}}^T \mathbf{K}_e \dot{\mathbf{e}} \leq \\ &\leq -\dot{\mathbf{E}}^T \mathbf{K}_D \dot{\mathbf{E}} - \dot{\mathbf{e}}^T \left(\lambda_{\min}\{\mathbf{K}_e\} - \left\| \mathbf{a} \mathbf{T} \left(\frac{1}{2} \dot{\mathbf{M}}(\mathbf{q}) - \mathbf{C}(\mathbf{q}, \dot{\mathbf{q}}) \right) \right\| \right) \dot{\mathbf{e}}. \end{aligned} \quad (41)$$

Since $\frac{1}{2} \dot{\mathbf{M}}(\mathbf{q}) - \mathbf{C}(\mathbf{q}, \dot{\mathbf{q}})$ is an oblique symmetric matrix, so $\dot{\mathbf{e}}^T \left(\frac{1}{2} \dot{\mathbf{M}}(\mathbf{q}) - \mathbf{C}(\mathbf{q}, \dot{\mathbf{q}}) \right) \dot{\mathbf{e}} = 0$. Since both $\dot{\mathbf{M}}(\mathbf{q})$ and $\mathbf{C}(\mathbf{q}, \dot{\mathbf{q}})$ satisfy the Lipschitz condition, then:

$$\left\| \mathbf{a} \mathbf{T} \left(\frac{1}{2} \dot{\mathbf{M}}(\mathbf{q}) - \mathbf{C}(\mathbf{q}, \dot{\mathbf{q}}) \right) \right\| \leq c_1 \|\mathbf{q}\| + c_2 \|\dot{\mathbf{q}}\|. \quad (42)$$

(41) can be written as following according to (42):

$$\dot{V} \leq -\dot{\mathbf{E}}^T \mathbf{K}_D \dot{\mathbf{E}} - \dot{\mathbf{e}}^T (\lambda_{\min}\{\mathbf{K}_e\} - c_1 \|\mathbf{q}\| + c_2 \|\dot{\mathbf{q}}\|) \dot{\mathbf{e}}. \quad (43)$$

If the \mathbf{K}_e compensation gain satisfies

$$\lambda_{\min}\{\mathbf{K}_e\} = C_1 \|\mathbf{q}\| + C_2 \|\dot{\mathbf{q}}\| \geq c_1 \|\mathbf{q}\| + c_2 \|\dot{\mathbf{q}}\|,$$

then $\dot{V} \leq 0$. Therefore, the L_2 norm of $\dot{\mathbf{E}}$ and $\dot{\mathbf{e}}$ is bounded.

Furtherly, according to (34) and (36), \ddot{E} and \ddot{e} are also bounded. Therefore, \dot{E} and \dot{e} are consistently continuous. According to Barbalat's theorem, $\dot{E} \rightarrow 0$ and $\dot{e} \rightarrow 0$ can be obtained when $t \rightarrow \infty$, and in line with (34), $\dot{q} \rightarrow 0$, $\ddot{q} \rightarrow 0$ can also be obtained when $t \rightarrow \infty$. According to (36), there is a constant set:

$$\psi = \{(q, \dot{q}) : q = 0, \dot{E} = 0, e = 0, \varepsilon = 0\}.$$

So, in compliance with the LaSalle theorem, the system is asymptotically stable, that is $e \rightarrow 0$ and $\varepsilon \rightarrow 0$ when $t \rightarrow \infty$. The controller of (35) can be written as a PD error feedback controller:

$$u_{\Delta} = K_P(I + aT)e + [K_D(I + aT) + (I + aT)^{-1}K_e] \dot{e} = \bar{K}_P e + \bar{K}_D \dot{e}. \quad (44)$$

Fig. 4 is the control block diagram of the system.

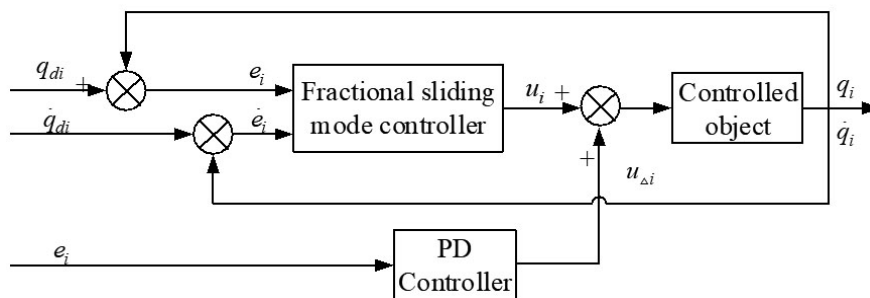


Fig. 4. Control block diagram of system

Fig. 5 is a schematic diagram of the structure of the three-joint manipulator.

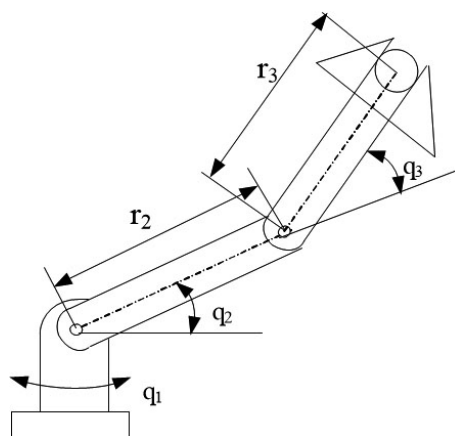


Fig. 5. Structure of the robotic arm

5.3. Simulation

The simulation object selects a three-joint industrial robot. According to the dynamic model derived above, the expressions of each matrix in the model can be written as:

$$\mathbf{C}(\mathbf{q}, \dot{\mathbf{q}}) = \begin{bmatrix} c_{11} & c_{12} & c_{13} \\ c_{21} & c_{22} & c_{23} \\ c_{31} & c_{32} & c_{33} \end{bmatrix}, \quad \mathbf{M}(\mathbf{q}) = \begin{bmatrix} m_{11} & m_{12} & m_{13} \\ m_{21} & m_{22} & m_{23} \\ m_{31} & m_{32} & m_{33} \end{bmatrix},$$

$$\mathbf{G}(\mathbf{q}) = [g_1 \ g_2 \ g_3]^T, \quad \mathbf{q} = [q_1 \ q_2 \ q_3]^T,$$

$$m_{11} = I_1 + a_1 \cos^2(q_2) + a_2 \cos^2(q_2 + q_3) + 2a_3 \cos(q_2) \cos(q_2 + q_3),$$

$$m_{12} = m_{21} = m_{13} = m_{31} = 0, \quad m_{22} = I_2 + a_1 + a_2 + 2a_3 \cos(q_3),$$

$$m_{23} = m_{32} = a_2 + a_3 \cos(q_3), \quad m_{33} = I_3 + a_2,$$

$$c_{11} = -\frac{1}{2}a_1\dot{q}_2 \sin(2q_2) - \frac{1}{2}a_2(\dot{q}_2 + \dot{q}_3) \sin(2q_2 + 2q_3) -$$

$$- a_3\dot{q}_2 \sin(2q_2 + q_3) - a_3\dot{q}_3 \cos(q_2) \sin(q_2 + q_3),$$

$$c_{12} = -\frac{1}{2}a_1\dot{q}_1 \sin(2q_2) - \frac{1}{2}a_2\dot{q}_1 \sin(2q_2 + 2q_3) - a_3\dot{q}_1 \sin(2q_2 + q_3),$$

$$c_{13} = -\frac{1}{2}a_1\dot{q}_1 \sin(2q_2 + 2q_3) - a_3\dot{q}_1 \cos(q_2) \sin(q_2 + q_3),$$

$$c_{21} = -c_{12}, \quad c_{31} = -c_{13}, \quad c_{33} = 0,$$

$$c_{22} = -a_3\dot{q}_3 \sin(q_3), \quad c_{23} = -a_3(\dot{q}_2 + \dot{q}_3) \sin(q_3), \quad c_{32} = -a_3\dot{q}_2 \sin(q_3),$$

$$g_1 = 0, \quad g_2 = b_1 \cos(q_2) + b_2 \cos(q_2 + q_3), \quad g_3 = b_2 \cos(q_2 + q_3),$$

where:

$$a_1 = m_2 r_2^2 + m_3 l_2^2, \quad a_2 = m_3 l_3^2, \quad a_3 = m_3 r_3 l_2, \quad b_1 = (m_2 r_2 + m_3 l_2)g, \quad b_2 = m_3 r_3 g.$$

Physical parameters are set as:

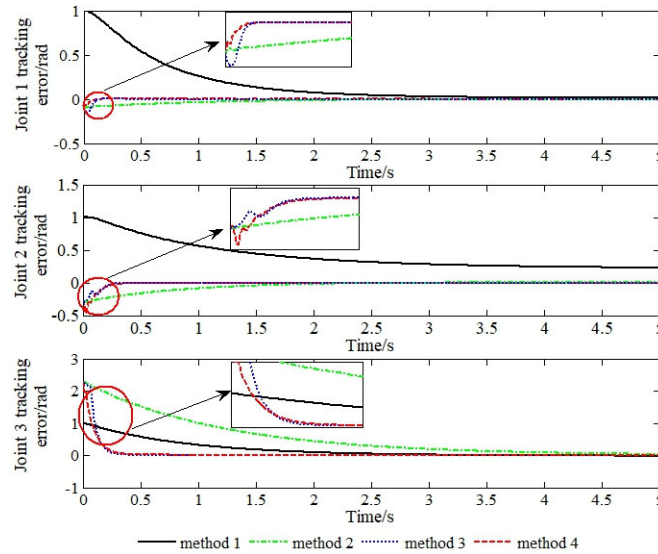
$$m_2 = 30 \text{ Kg}, \quad m_3 = 26 \text{ Kg}, \quad r_2 = 0.6 \text{ m}, \quad r_3 = 0.5 \text{ m}, \quad g = 9.8 \text{ m/s}^2, \quad I_1 = 3.61 \text{ Kg} \cdot \text{m}^2,$$

$$I_2 = 2.35 \text{ Kg} \cdot \text{m}^2, \quad I_3 = 1.95 \text{ Kg} \cdot \text{m}^2.$$

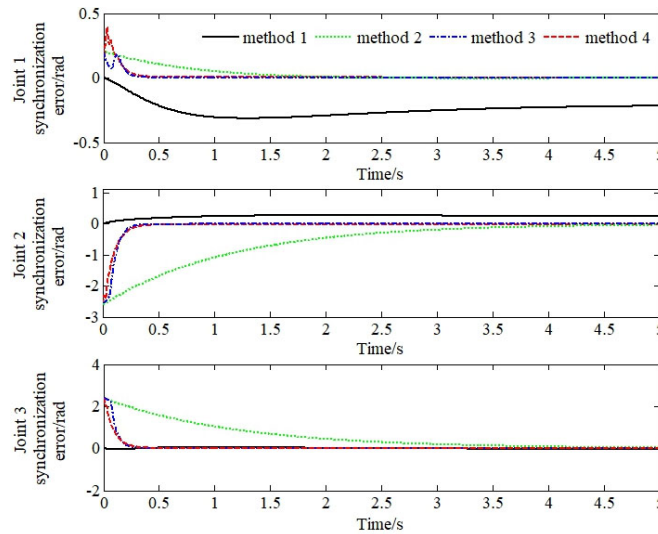
The following control methods are used to compare and analyze the simulation method 1: PD cross-coupling control; method 2: PD iterative cross-coupling control; method 3: fractional sliding mode cross-coupling control; method 4: fractional-order iterative sliding mode cross-coupling control.

The desired trajectory is set as a step signal, the system has no disturbance, and the number of iterations is 10. Fig. 6 shows the position tracking error and synchronization error curve of the three-joint robot under the above four methods. Table 3 shows the comparison of the data under different control methods, where the root mean square error of the angular displacement adjustment time and position error are chosen as the reference values of the comparison.

It can be seen from Fig. 6 and Table 3 that when there is no disturbance in the system, the control strategy designed in this paper can help one to achieve the goal of synchronous



(a) Position tracking error curve



(b) Synchronous error curve

Fig. 6. Position tracking error and synchronization error curve of three-joint robot

control more successfully, which can effectively shorten the time of the angular displacement adjustment of the joint. At the same time, the convergence speed of the system position error is obviously accelerated, the root mean square error of the single joint synchronization error and the position error are obviously reduced, the convergence effect is also obviously enhanced, and the synchronization effect of the system becomes better.

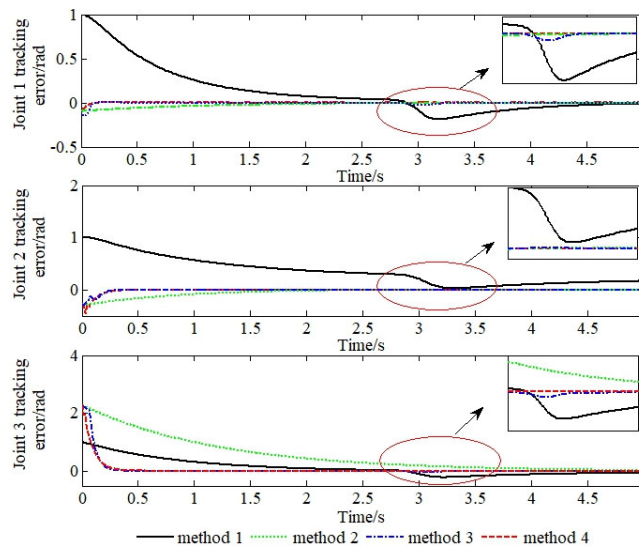
Table 3. Comparison of data between different control methods

| | Method 1 | Method 2 | Method 3 | Method 4 |
|--|----------|-----------------------|-----------------------|-----------------------|
| Joint 1 angular displacement adjustment time (s) | 3.25 | 2.85 | 0.14 | 0.11 |
| Joint 2 angular displacement adjustment time (s) | > 5 | 2.32 | 0.33 | 0.31 |
| Joint 3 angular displacement adjustment time (s) | 3.15 | 4.22 | 0.28 | 0.24 |
| Root mean square error of position error of joint 1 after 2 s (rad) | 0.1527 | 7.02×10^{-3} | 3.23×10^{-5} | 6.47×10^{-6} |
| Root mean square error of position error of joint 2 after 2 s (rad) | 0.3853 | 1.21×10^{-2} | 5.59×10^{-4} | 3.69×10^{-4} |
| Root mean square error of position error of joint 3 after 2 s (rad) | 0.2789 | 0.1182 | 8.05×10^{-3} | 6.91×10^{-3} |
| Root mean square error of synchronization error of joint 3 after 2 s (rad) | 0.2559 | 2.29×10^{-2} | 2.62×10^{-3} | 1.36×10^{-3} |
| Root mean square error of synchronization error of joint 3 after 2 s (rad) | 0.3431 | 0.2251 | 8.89×10^{-3} | 7.81×10^{-3} |

Take uncertain disturbance into the system, that is:

$$f(t) = 1000 \exp(-(t - 3)^2 / (2 \times 0.1^2)).$$

The following results can be obtained. Fig. 7 shows the position tracking error curve and synchronization error curve of the three-joint robot under different control methods with the disturbance term.



(a) Position tracking error curve

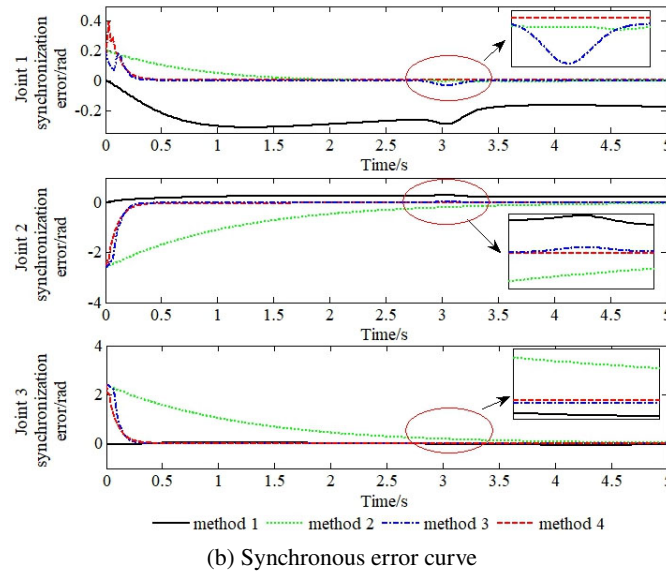


Fig. 7. Position tracking error and synchronization error curve of three-joint robot

It can be obtained from Fig. 6 and Fig. 7 that when there is disturbance in the system, the control strategy proposed in the paper is more helpful than other synchronous control methods with better anti-jamming. In order to further verify the control performance of the proposed method, a sinusoidal signal is selected as the desired trajectory, which is:

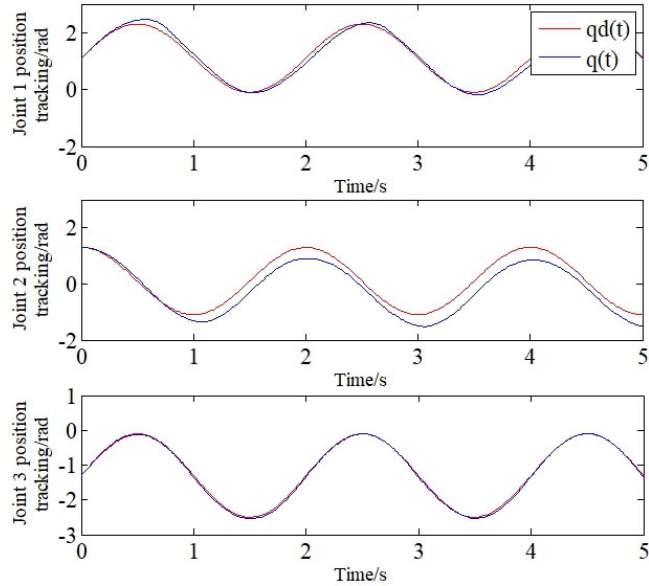
$$\begin{aligned}
 q_{1d} &= 1.1 + 1.2 \sin \pi t, \\
 q_{2d} &= 0.1 + 1.2 \cos \pi t, \\
 q_{3d} &= -1.3 + 1.2 \sin \pi t, \\
 \mathbf{q}(0) &= [1.1 \ 1.3 \ -1.3]^T, \\
 \dot{\mathbf{q}}(0) &= [1.2\pi \ 0 \ 1.2\pi]^T.
 \end{aligned}$$

The following results are obtained.

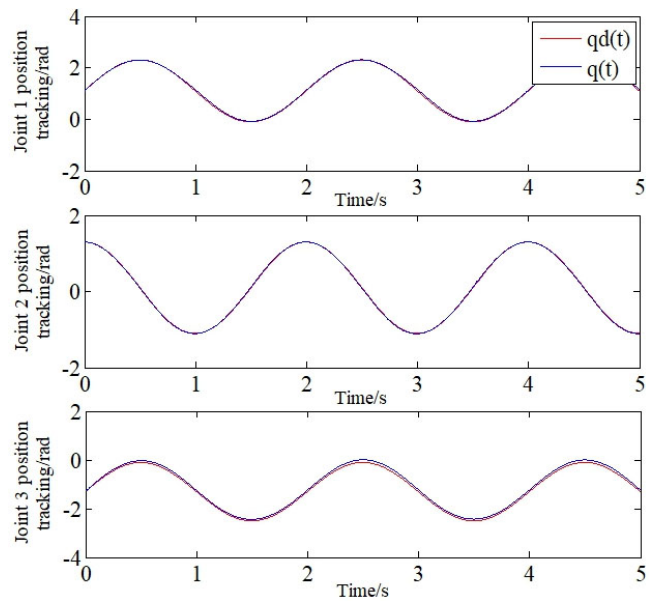
Fig. 8 shows the position trajectory tracking curves of each joint under method 1 and method 3. Fig. 9(a) and (b) are the 10 iterative position trajectory tracking curves of each joint under method 2, (c) and (d) are the 10 iterative position trajectory tracking curves of each joint under method 4.

It can be seen from the comparison between Fig. 8 and Fig. 9 that when the iterative learning control algorithm is adopted, the system can achieve complete tracking, and the fractional sliding mode control is better than the PD control tracking. Under the control strategy designed in this paper, the tracking speed and tracking effect of each joint are significantly improved, and the ability to deal with uncertain disturbances is better.

Fig. 10 shows the maximum absolute value convergence curve of the position (speed) error of the third joint of the methods 2 and 4. The comparison can be concluded as follows: the absolute



(a) Position tracking error curve

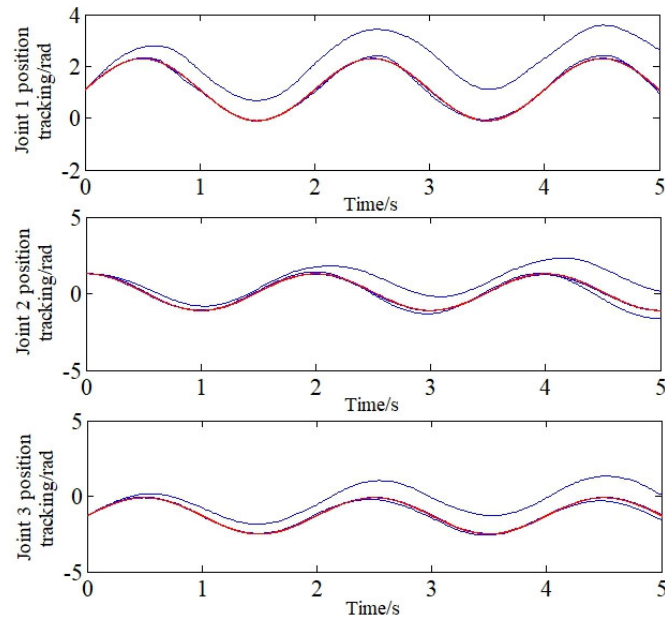


(b) Method 3 position tracking curve

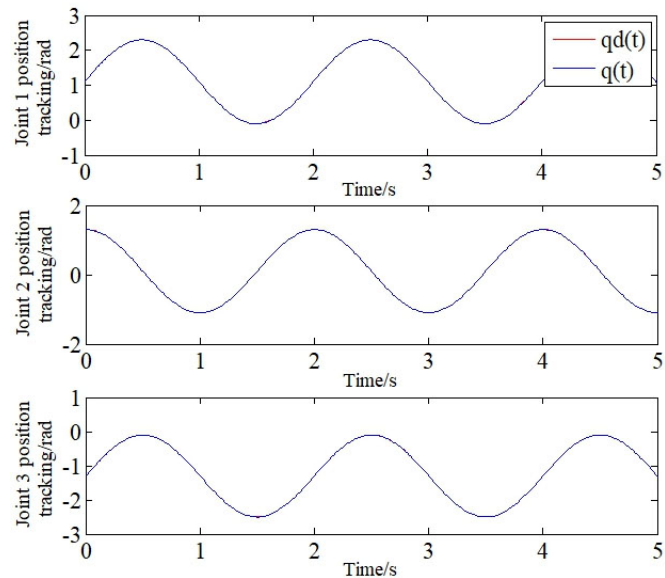
Fig. 8. Position trajectory tracking curve of each joint under method 1 and method 3

values of the position error of the three joints are maxima of 0.0761, 0.0253, 0.1115 in method 4, while they are 1.5352, 1.5547, 1.4736 in method 2; the absolute values of the speed error are

0.2963, 0.0786, 0.4902 in method 4 while they are 1.4575, 1.8365, 0.8826 in method 2. Therefore, from the overall point of view, the error of the position and speed of the method proposed in the paper is smaller than that of method 4 and the control precision is higher.

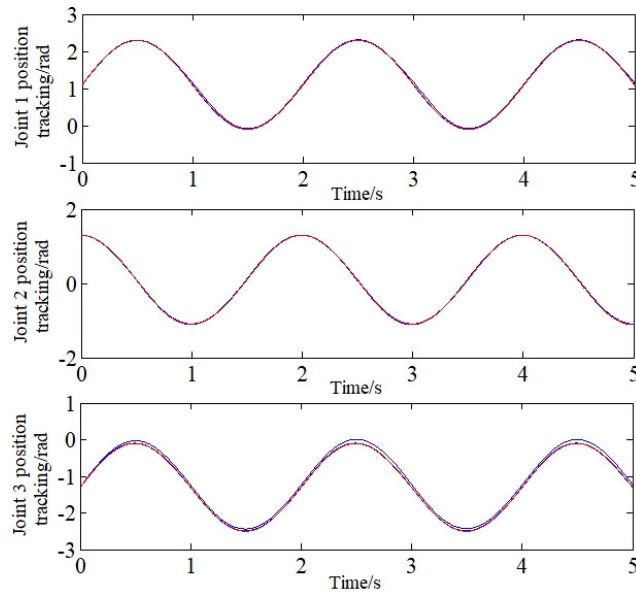


(a) 10-th iteration position tracking curves

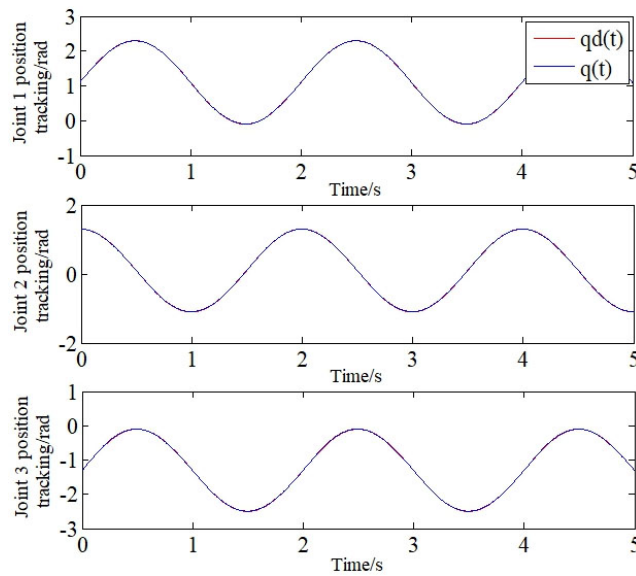


(b) 10-th iteration position tracking curves

In order to verify the control performance of the control algorithm designed in this paper, the trajectory tracking experiment was performed on the first three joints of the GRB4016 robotic arm, and the other joints were locked. The experimental platform is a 6-DOF robot arm



(c) 10-th iteration position tracking curves



(d) 10-th iteration position tracking curves

Fig. 9. The trajectory tracking curve of 10 iterations of each joint of method 2 and method 4

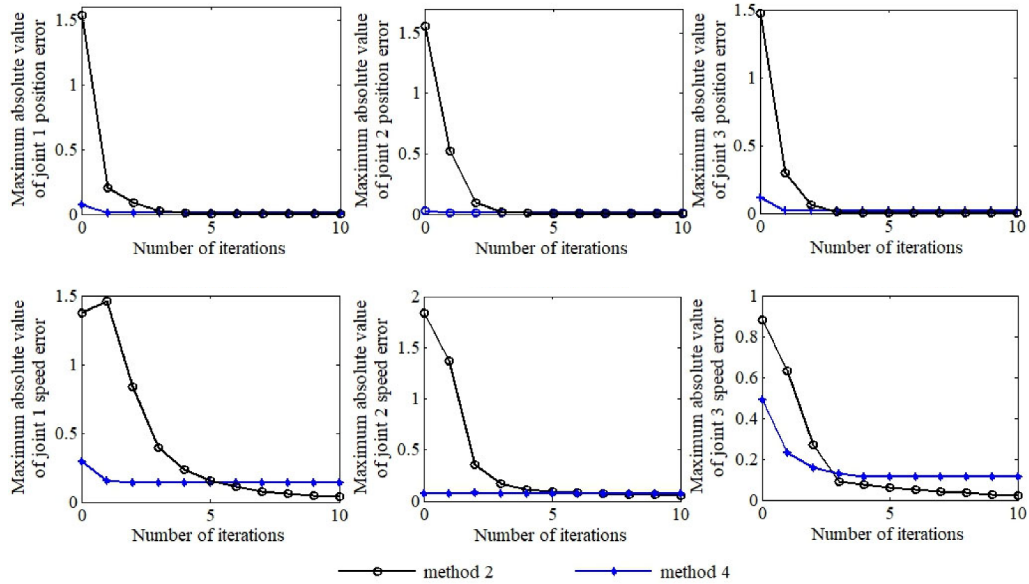


Fig. 10. Three-joint position (speed) error maximum absolute value convergence process

developed by Gugao Company. The control system is shown in Fig. 11. The system control process: measuring the angular position of the joint motor, transmitting it to the data acquisition module of the robot electric control cabinet through a dedicated cable, and then transmitting it to the computer through RS232, calculating the output control torque through the host computer controller, and sending it to the driver through the data acquisition module. Driving the arm joint motor movement to complete the robot arm control task. The experimental results are shown in Fig. 12, which verifies the effectiveness of the control strategy designed in this paper.

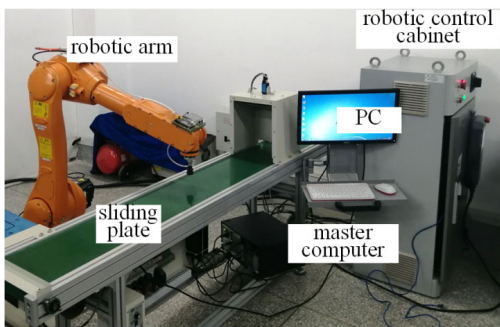


Fig. 11. Experimental platform

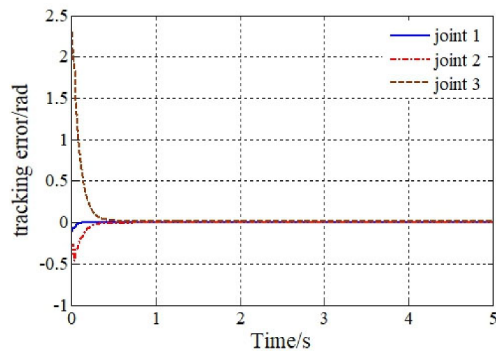


Fig. 12. Tracking error curves of joints

6. Conclusions

In order to improve the accuracy of tracking and synchronization of the joint motion of each arm, the position tracking control strategy of a single-joint manipulator and the fractional-order iterative sliding mode cross-coupling control strategy of a multi-joint manipulator were proposed, based on the idea of combining fractional calculus with sliding mode control and iterative learning control. The final conclusions are as follows:

1. Single joint position control is the precondition for realizing multi-joint synchronization control. This paper proposes a fractional-order iterative sliding mode control strategy based on the combination of fractional calculus, iterative learning control and sliding mode control to improve the tracking speed and tracking of a single joint. Taken the position tracking, control input and position (speed) error maximum absolute value convergence process as a basis for judging, which can be obtained by the comparison of the fractional sliding mode control strategy and integer order iterative sliding mode control strategy, this method has better tracking effect and robustness, as well as the system chatter is smaller.
2. In this paper, the fractional-order iterative sliding mode cross-coupling control strategy was adopted to eliminate the synchronization error between multiple joints. Compared with PD cross-coupling control strategy, PD iterative cross-coupling control strategy, and fractional-order sliding mode control strategy, the fractional order iterative sliding mode cross-coupling control strategy designed in this paper has smaller angular displacement adjustment time and root mean square error, so it is synchronized. The error convergence is faster, the dispersion is small, and the synchronization accuracy is satisfied.

References

- [1] Shi X.P., Liu S.R., *A survey of trajectory tracking control for robot manipulators*, Control Engineering of China, vol. 18, no. 1, pp. 116–122 (2011).
- [2] Liu J.K., *Design of robot control system and MATLAB simulation*, Tsinghua University press (2008).
- [3] Hu S.B., *Sliding mode control of nonlinear multi joint robot system*, National Defense Industry Press (2015).
- [4] Chen Q., Luo P., *Adaptive sliding mode control for electromechanical servo system with saturation compensation based on extended state observer*, Journal of Systems Science and Mathematical Sciences, vol. 36, no. 10, pp. 1535–1547 (2016).
- [5] Li W.L., Shi X.H., Ke J., *Engine torque pulsation simulation under idling speed based on sliding mode and iterative learning control*, Journal of Vibration Measurement and Diagnosis, vol. 36, no. 2, pp. 359–365 (2016).
- [6] Yan L.Y., Ye P.Q., Zhang H., *Disturbance rejection for linear motor based on multi-periodic learning variable structure control*, Electric Machines and Control, vol. 21, no. 1, pp. 8–13 (2017).
- [7] Zhang Z., Ye D., Sun Z.W., *Sliding mode fault tolerant attitude control for satellite based on iterative learning observer*, Journal of National University of Defense Technology, vol. 40, no. 1, pp. 17–23 (2018).
- [8] Matusiak M., Ostalczyk P., *Problems in solving fractional differential equations in a microcontroller implementation of an FOPID controller*, Archives of Electrical Engineering, vol. 68, no. 3, pp. 565–577 (2019).

- [9] Yin C., Cheng Y., Zhong S.M., *Fractional-order sliding mode-extremum seeking control design with fractional-order PI sliding surface*, Control Conference, IEEE, pp. 539–544 (2015).
- [10] Zhang K.J., Peng G.H., Dou J.J., *Robustness of PD δ type iterative learning control for fractional-order linear time-delay systems*, Science Technology and Engineering, vol. 453, no. 20, pp. 135–139 (2018).
- [11] Song S.M., Deng L.W., Chen X.L., *Application characteristics of fractional calculus in sliding mode control*, Journal of Chinese Inertial Technology, vol. 22, no. 4, pp. 439–444 (2014).
- [12] Koren Y., *Cross-coupled biaxial computer controls for manufacturing systems*, Journal of Dynamic Systems Measurement and Control, vol. 102, no. 4, pp. 265–272 (1980).
- [13] Xu W., Hou J., Yang W., Wang C., *A double-iterative learning and cross-coupling control design for high-precision motion control*, Archives of Electrical Engineering, vol. 68, no. 2, pp. 427–442 (2019).
- [14] Chu T.T., *Research on robotic high precision tracking based on multi-axial coupling synchronized control*, Harbin Institute of Technology (2015).
- [15] Zhong G., Shao Z., Deng H., *Precise position synchronous control for multi-axis servo systems*, IEEE Transactions on Industrial Electronics, vol. 64, no. 5, pp. 3707–3717 (2017).
- [16] Delavari H., Baleanu D., Sadati J., *Stability analysis of caputo fractional-order nonlinear systems revisited*, Nonlinear Dynamics, vol. 67, no. 4, pp. 2433–2439 (2012).
- [17] Dadras S., Momeni H.R., *Fractional terminal sliding mode control design for a class of dynamical systems with uncertainty*, Communications in Nonlinear Science and Numerical Simulation (S1007-5704), vol. 17, no. 1, pp. 367–377 (2012).
- [18] Devika K.B., Thomas S., *Power rate exponential reaching law for enhanced performance of sliding mode control*, International Journal of Control, Automation and System, vol. 15, no. 6, pp. 2636–2645 (2017).
- [19] Umarov S., *Introduction to fractional and pseudo-differential equations with singular symbols*, Springer International Publishing (2015).
- [20] Benito F.M., Rolando R., Anthony T., Carlos F., *Application of fractional calculus to oil industry*, Intech (2017).
- [21] Li Y., Chen Y.Q., Podlubny I., *Technical communique: mittag-leffler stability of fractional order nonlinear dynamic systems*, Automatica (S0005-1098), vol. 45, no. 8, pp. 1965–1969 (2009).
- [22] Tepljakov A., Petlenkov E., Belikov J., *FOMCON: fractional-order modeling and control toolbox for MATLAB*, International Conference Mixed Design of Integrated Circuits and Systems – Mixdes, IEEE, pp. 684–689 (2011).